1   Respiratory heterogeneity shapes biofilm formation and host colonization in

2   uropathogenic *Escherichia coli*

3

4   Running title: Respiratory heterogeneity in uropathogenic *Escherichia coli*

5

6   Connor J. Beebout,[a] Allison R. Eberly,[a] Sabrina H. Werby,[b] Seth A. Reasoner,[a] John R.

7   Brannon,[a] Shuvro De,[c] Madison J. Fitzgerald,[d] Marissa M. Huggins,[d] Douglass B.

8   Clayton,[c] Lynette Cegelski,[b] and Maria Hadjifrangiskou[a,e]#

9

10   [a]Department of Pathology, Microbiology, and Immunology, Vanderbilt University

11   Medical Center, Nashville, TN, USA

12   [b]Department of Chemistry, Stanford University, Stanford, CA, USA

13   [c]Division of Pediatric Urology, Vanderbilt University Medical Center, Nashville, TN, USA

14   [d]Vanderbilt University, Nashville, TN, USA

15   [e]Vanderbilt Institute for Infection, Immunology & Inflammation, Vanderbilt University

16   Medical Center, Nashville, TN, USA

17

18   #Address correspondence to: maria.hadjifrangiskou@vumc.org, @BacterialTalk

19

Abstract

Biofilms are multicellular bacterial communities encased in a self-secreted extracellular matrix comprised of polysaccharides, proteinaceous fibers, and DNA. Organization of these components lends spatial organization to the biofilm community such that biofilm residents can benefit from the production of common goods, while being protected from exogenous insults. Spatial organization is driven by the presence of chemical gradients, such as oxygen. Here we quantified and localized the expression of two *Escherichia coli* cytochrome oxidases in cells found in the biofilm state and defined their contribution to biofilm architecture. These studies elucidated a role for the high-affinity quinol oxidase cytochrome *bd* in matrix production and biofilm resident protection. Cytochrome *bd* was the most abundantly expressed respiratory complex in the biofilm community and was localized in the biofilm interior. Depletion of the cytochrome *bd*-expressing subpopulation led to decreased extracellular matrix and increased sensitivity of the community to exogenous stresses. Interrogation of the distribution of cytochrome oxidases in the planktonic state revealed that ~15% of the population expresses cytochrome *bd* at atmospheric oxygen concentration, and this population dominates during acute urinary tract infection. These data point towards a bet-hedging mechanism in which heterogeneous expression of respiratory complexes ensures respiratory plasticity of *E. coli* across diverse host niches.

Keywords

biofilms, heterogeneity, oxygen gradients, respiration, urinary tract infection

Importance

Biofilms are multicellular bacterial communities encased in a self-secreted extracellular matrix comprised of polysaccharides, proteinaceous fibers, and DNA. Organization of these components lends spatial organization in the biofilm community. Here we demonstrate that oxygen gradients in uropathogenic *Escherichia coli* (UPEC) biofilms lead to spatially distinct expression programs for cytochrome oxidases – components of the terminal electron transport chain. Our studies reveal that the cytochrome *bd*-expressing subpopulation is critical for biofilm development and matrix production. In addition, we show that cytochrome oxidases are also heterogeneously expressed in planktonic populations, and that this respiratory heterogeneity provides a fitness advantage during infection. These studies define the contributions of cytochrome oxidases to biofilm physiology and suggest the presence of respiratory bet-hedging behavior in UPEC.

Introduction

Rather than existing as a phenotypically uniform population, bacterial communities are characterized by subpopulations that are oftentimes phenotypically distinct. This intra-strain heterogeneity can be transient, brought about by stochastic differences in the abundance and activity of regulators in each individual cell, or it can be irreversible, through the acquisition of mutations. Heterogeneity influences the fate of the particular strain by allowing for at least a portion of the population to thrive in different niches as a result of its specific expression program.

64   Biofilms are complex multicellular communities assembled in an organized

65   fashion in three-dimensional space. One of the most critical features of biofilms is a self-

66   secreted extracellular matrix (ECM) that comprises a variety of exopolysaccharides,

67   proteinaceous fibers, and extracellular DNA (1). The ECM protects the biofilm residents

68   from predation, desiccation, assault by antimicrobial agents, and, when biofilms form in

69   the host, the immune system. In addition to providing a physical barrier against external

70   threats, the ECM also serves as a barrier to diffusion. Restricted diffusion, in

71   conjunction with the metabolic activity of resident bacteria, leads to the establishment of

72   various chemical gradients throughout the biofilm community (2, 3). Bacteria at different

73   locales along the gradient respond to the microenvironment differently, and as a result

74   differentiate into distinct and often metabolically cooperative subpopulations (3-7).

75   Previous studies in *Pseudomonas aeruginosa* and *Escherichia coli* indicated that

76   oxygen gradients play a key role in regulating the differential expression of genes

77   involved in biofilm formation and metabolic specialization (8-11). The presence of an

78   oxygen gradient suggests the emergence of subpopulations that utilize different

79   respiratory components as a function of the oxygen abundance to which they are

80   exposed. This leads to the hypothesis that the metabolic program of differentially

81   respiring subpopulations is distinct from one another and contributes to differential

82   production of biofilm goods that in turn enhance biofilm resilience.

83   *Escherichia coli* is a facultative anaerobe capable of utilizing multiple metabolic

84   pathways to fulfill its energy requirements. In aerobically respiring *E. coli*, cytochrome

85   oxidases comprise essential components of the terminal electron transport chain that

86   couple the flow of electrons to the reduction of molecular oxygen into water (12, 13). *E.*

87 *coli* encodes two classes of cytochrome oxidases with differing oxygen affinities: one

88 heme copper oxidase, cytochrome *bo* (encoded by the *cyoABCD* gene cluster), and two

89 *bd*-type oxidases, cytochromes *bd* (*cydABX*) and bd_2 (*appBC*) (13, 14). Cytochrome *bo*

90 is induced at high (atmospheric, 21%) oxygen tensions, whereas the *bd*-type oxidases

91 are induced at low (hypoxic, 2-15%) oxygen tensions (13, 15). Based on these *in vitro*

92 expression patterns, we hypothesized that cytochrome *bo* would be enriched on the air-

93 exposed biofilm surface, whereas cytochromes *bd* and bd_2 would be enriched in the

94 hypoxic interior.

95   Here we report that the spatial distribution of cytochrome oxidases in biofilms

96 formed by uropathogenic *Escherichia coli* (UPEC) is a fundamental driver of biofilm

97 architecture. Peptide nucleic acid fluorescence *in situ* hybridization (PNA-FISH)

98 analyses assigned locations to each cytochrome-producing subpopulation, elucidating

99 for the first time spatially distinct expression programs for respiratory oxidases in *E. coli*.

100 Depletion of the cytochrome *bd*-expressing subpopulation from the biofilm significantly

101 impaired diffusion resistance by altering the abundance and organization of the ECM.

102 Assessment of deletion mutants in a well-established urinary tract infection murine

103 model revealed that only the cytochrome *bd* mutant was significantly attenuated for

104 virulence, although the infecting pool of bacteria in the parent strain exhibited

105 heterogeneous expression of all three respiratory oxidases. *In situ* analysis of urine-

106 associated bacteria demonstrated a shift of the population to cytochrome *bd* expression,

107 suggesting that the bladder favors cytochrome *bd*-expressing bacteria and that

108 heterogeneity in the input pool provides a fitness advantage to uropathogenic strains.

109 Our studies, performed on one of the most commonly acquired human pathogens and a

110   prolific biofilm producer *in vivo*, unveil a potential avenue for targeting heterogeneity and

111   homogenizing bacterial programming as a therapeutic approach.

112

113   **Results**

114   *Cytochrome bd is the most abundant respiratory transcript in mature UPEC biofilms*

115   To test the hypothesis that multiple differentially respiring subpopulations exist in *E. coli*

116   biofilms, we measured the relative expression of components of the aerobic (*cyoABCD*,

117   *appBC*, and *cydABX*) and anaerobic (*napABC* and *narGHI*) respiratory chains in mature

118   colony biofilms. Previous studies demonstrated that the central and peripheral regions

119   of biofilms are metabolically distinct, yet co-dependent (16). The central region is

120   shielded from environmental stressors and is therefore critical for survival of the

121   population. The peripheral region contains a rapidly expanding population that

122   contributes most to biofilm growth at the expense of being highly susceptible to

123   exogenous threats. We first analyzed transcript levels in the center and periphery of

124   colony biofilms grown on Yeast Extract/Casamino Acids (YESCA) agar (Fig. 1a), a

125   medium which induces expression of key matrix components (curli amyloid fibers, type

126   1 pili, secreted proteins Hu-α/β, cellulose) that are also critical for fitness in the urinary

127   tract (10, 17-19). At both regions, of the five respiratory operons analyzed, over 90

128   percent of transcripts corresponded to aerobic respiratory components (Fig. 1b-c). The

129   most abundant transcript was that of *cydA* (Fig. 1b-d), corresponding to cytochrome *bd*

130   complex (*cydABX*) expression. The *cydA* transcript levels were approximately 2-fold

131   higher than those corresponding to *cyoABCD* (Fig. 1b-d), which was the second most

132   highly abundant oxidase under the conditions tested. Cytochrome bd_2 was the third

6

133   most-highly expressed, while the anaerobic *narG* and *napA* genes exhibited baseline

134   expression levels (Fig. 1b-d). These results validated that most of the biofilm is hypoxic,

135   consistent with previous work in *P. aeruginosa* and *E. coli* (8, 9).

136

137   _Spatial organization of cytochrome expression along the oxygen gradient_

138   Previous studies elucidated the presence of steep biofilm oxygen gradients as a

139   function of biofilm depth (Fig. 2a) (8, 9). To define the spatial distribution of cytochrome-

140   expressing subpopulations, we performed PNA-FISH on cryosections of mature colony

141   biofilms using probes targeting each cytochrome oxidase operon (*cyoA*, *appC*, and

142   *cydA*) as well as *rrsH* as an endogenous control. Each PNA-FISH probe was designed

143   using the validated probe sequences used for qPCR (Fig. 1 and Table S1) to ensure

144   comparable hybridization efficiencies for each probe. SYTO 9 staining of sections was

145   used as an additional control to localize the entire biofilm community and account for

146   possible hybridization inconsistencies with the *rrsH* control probe (Figs. 2d, j and S1).

147   Consistent   with   previous   observations   demonstrating   that   the   highest   oxygen

148   abundance is at the air-exposed surface of the biomass (8, 9), we observed that

149   *cyoABCD* transcript was most abundant in bacteria lining the air-exposed surface of the

150   biofilm (Fig. 2b-c, f, h-i, l, n). In contrast, the highest abundance of *cydABX* transcript

151   was found in densely packed clusters of bacteria in the interior of the biofilm (Fig. 2b-c,

152   e, g, i, k, m). Interestingly, while in K12 *E. coli* the function of cytochrome *bd* and *bd*$_2$ are

153   thought to be redundant, the expression distribution of the two gene clusters was

154   different, with *appBC* observed to be evenly distributed throughout the community (Fig.

155   S1).

7

156

157 *Loss of cytochrome bd alters biofilm architecture, development, and matrix abundance*

158 The highly regulated spatial expression of cytochrome *bo* and cytochrome *bd*

159 oxidases in the biofilm raised the hypothesis that each of these cytochrome-expressing

160 subpopulations uniquely contributes to overall biofilm architecture. To test this

161 hypothesis, we created isogenic deletion mutants lacking the *cyoAB*, *appBC*, or *cydAB*

162 genes and compared the biofilms formed by the resulting strains (Fig. 3a). Colony

163 biofilms formed by the parental strain expand to an average diameter of 16.8 mm over

164 an 11-day incubation period and exhibit elaborate rugose architecture with distinct

165 central and peripheral regions (Figs. 3a and S2). Strains deleted for *cyoAB* and *appBC*

166 exhibited inverse phenotypes to each other, with the Δ*cyoAB* colony biofilms expanding

167 more than the parental strain (average diameter: 19.9 mm) and the Δ*appBC* colony

168 biofilms appearing more compact and with apparently higher rugosity (Figs. 3a and S2).

169 Strikingly, while Δ*cyoAB* and Δ*appBC* only displayed minor architectural changes,

170 Δ*cydAB* colony biofilms exhibited pronounced defects both in development and

171 architecture (Fig. 3a and S2). Colonies deleted for *cydAB* grew at a similar rate as the

172 parent, Δ*cyoAB*, and Δ*appBC* for the first 72 hours (Fig. S2). However, colony growth

173 was significantly stunted between days 3 and 11, with radial expansion remaining at an

174 average diameter of 10.3 mm and colonies exhibiting a wet mass of 48.11 mg (70% of

175 the parent strain) at the end of the experiment, even though the CFU produced by the

176 two strains were comparable across the 11-day incubation period (Figs. 3b-c and S2).

177 Complementation of Δ*cydAB* with an extra-chromosomal construct expressing *cydABX*

178 under its native promoter rescued the deletion phenotype, indicating that the defects

8

179 observed in the Δ*cydAB* mutant stem solely from the removal of the *cydABX* cluster

180 (Fig. S3). Together, these observations demonstrate that cytochrome *bd* is a key

181 contributor to biofilm development and suggest that loss of *cydAB* alters the synthesis

182 and organization of the ECM.

183   Under the conditions used, the ECM of *E. coli* comprises primarily of cellulose

184 and curli amyloid fibers (20). Previous solid-state nuclear magnetic resonance (NMR)

185 spectroscopy analyses on intact ECM material defined the contributions of cellulose and

186 curli to the *E. coli* biofilm ECM, and determined that curli and cellulose are present in a

187 6 to 1 ratio (20). More recently, the ECM cellulose was determined to be a chemically

188 modified form of cellulose, specifically phosphoethanolamine (pEtN) cellulose (21). To

189 interrogate the effects of *cydAB* deletion on curli and exopolysaccharide production, we

190 extracted ECM and performed solid-state NMR analysis to evaluate the abundance of

191 curli and cellulose components (Fig. 3d-e). The NMR spectra obtained for the parent

192 and Δ*cydAB* ECM are very similar overall, indicating a comparable protein to

193 polysaccharide ratio between the samples (Fig. 3d). Consistent with this analysis, we

194 observe no change in protein composition between the parent and Δ*cydAB* ECM

195 samples when analyzed on SDS-PAGE gels (Fig. 3e). We additionally do not observe

196 any overt alterations to curli abundance or localization between UTI89 and Δ*cydAB*

197 biofilm cryosections using immunofluorescence (Fig. 3f). Despite the similar

198 composition, the total amount of ECM recovered was reduced in Δ*cydAB*, indicative of a

199 decrease in ECM production. Because the protein to polysaccharide ratio and curli

200 abundance are unchanged between the parent and Δ*cydAB*, these data are suggestive

201 of a change to the overall mixture of matrix components in Δ*cydAB*, with particular

202 reductions in the abundance of non-curli and non-pEtN cellulose ECM components.

203   The ECM plays a central role in biofilm physiology by providing physical

204 protection against exogenous insults, serving as a structural scaffold, and helping to

205 establish chemical gradients which lead to metabolic differentiation and subpopulation

206 formation (2, 3, 17, 22). As such, disruptions to the matrix can have catastrophic

207 consequences for the biofilm community. We hypothesized that the altered matrix

208 abundance and architecture in the Δ*cydAB* mutant would render the biofilm more

209 susceptible to exogenous insults. To investigate this possibility, we probed the barrier

210 function of the cytochrome oxidase mutant biofilms by applying a drop of colored water

211 to the surface of mature colony biofilms (Fig. 3g and Movies S1-4) (23). While the

212 parent strain, Δ*cyoAB*, and Δ*appBC* biofilms repelled the drop, the solution readily

213 penetrated Δ*cydAB* biofilms, demonstrating that the alterations to Δ*cydAB* biofilm

214 architecture and matrix abundance increases penetrance of aqueous solutions.

215

216 *Loss of cytochrome bd increases population sensitivity to nitrosative stress under*

217 *ambient oxygen concentrations*

218   Together, our studies indicate that cytochrome *bd* is highly expressed in biofilms,

219 and that loss of the cytochrome *bd*-expressing subpopulation impairs barrier function

220 and reduces the abundance of extracellular matrix. These data suggest that the

221 cytochrome *bd*-expressing subpopulation plays a critical role in promoting ECM

222 synthesis and providing structural integrity to the community. However, it is also

10

223   possible that cytochrome *bd* is preferentially expressed in the biofilm because

224   cytochrome *bd* provides protection against oxidative and nitrosative stress – byproducts

225   of biofilm metabolism (24, 25) and, in the case of infection, components of the innate

226   immune response (26-28). Previous studies demonstrated that cytochrome *bd* has

227   catalase activity, is capable of oxidizing the respiratory inhibitor nitric oxide, and is

228   insensitive to nitrosative stress due to its unusually fast nitric oxide dissociation rate

229   (26). These biochemical activities are thought to occur at unique locations on the

230   protein; quinol oxidation occurs at the periplasmic Q loop, oxygen reduction and nitric

231   oxide binding occurs at heme *d*, and catalase activity is thought to occur through heme

232   b_{595} (14, 29, 30). By contrast, cytochrome *bo* affords no protection against oxidative or

233   nitrosative stress and is irreversibly inhibited by nitric oxide (26). Given these additional

234   functions of cytochrome *bd*, we performed growth curves at ambient oxygen

235   concentration and evaluated the effects of nitrosative and oxidative stress on the fitness

236   of cells lacking *cydAB* or *cyoAB* as compared to the parent strain. Without the addition

237   of stress, both mutants exhibited a lag in growth (Fig. 4a), but each reached a maximal

238   CFU/mL similar to the parental strain by the end of the growth experiment (Fig. 4a).

239   ATP measurements of the corresponding cultures revealed no significant overall

240   differences in ATP concentrations between the strains during logarithmic growth (Fig.

241   4b). Next, to determine whether loss of cytochrome *bd* impairs resistance to oxidative

242   and nitrosative stress, we measured growth with and without these stressors. Whereas

243   treatment with H_2O_2 had no significant effects on the growth of the two mutants (Fig.

244   4c), addition of the nitric oxide donor NOC-12 to planktonic cultures most significantly

245   impacted growth of Δ*cydAB* (Fig. 4d), consistent with previous studies on K12 *E. coli*

246 and the multi-drug resistant strain ST131 (27, 28). Together, these data demonstrate

247 that while cytochrome *bd* is dispensable for energy generation during planktonic growth,

248 loss of cytochrome *bd* sensitizes bacteria to nitrosative stress. In conjunction with the

249 disrupted biofilm architecture and altered matrix abundance in Δ*cydAB* biofilms, these

250 data suggest that cytochrome *bd*-expressing subpopulations are critical, not only for

251 directing matrix biosynthesis, but also for withstanding harmful metabolic byproducts

252 while in the biofilm state.

253

254 *Heterogeneous expression of cytochrome oxidases at the population level*

255   Our data thus far indicate that in addition to heterogeneity in cytochrome oxidase

256 expression in the biofilm state, heterogeneous expression of cytochrome oxidases must

257 also be occurring in the planktonic population. Our planktonic studies revealed a lag in

258 growth of the Δ*cyoAB* and the Δ*cydAB* mutants when these strains were grown under

259 ambient oxygen concentrations, suggesting that in a given culture there are

260 subpopulations – like in the biofilm – that stochastically or deterministically express

261 different respiratory components. Such a bet-hedging approach could provide UPEC

262 with the flexibility to quickly adapt to a given niche, be it different locales in the

263 genitourinary tract or in the gastrointestinal tract during host colonization. In the context

264 of urinary tract infection, *E. coli* traverse from the nearly anoxic gut to the perineum,

265 where it encounters atmospheric oxygen concentrations, prior to ascending the urethra

266 to enter the hypoxic bladder, where the dissolved urinary oxygen concentration is 4 –

267 6% (31). This microbial journey is performed by planktonic cells, which can then expand

268 into multicellular communities on and within bladder epithelial cells, as well as on

269 urinary catheters (1, 32). In previous studies, we and others demonstrated that UPEC

270 respire aerobically during infection (33-35) and that biofilm formation is favored in

271 conditions that mimic oxygen levels in the bladder (36).

272   The high abundance of *cydABX* transcript in the hypoxic areas of the biofilm, in

273 conjunction with the defects observed in aerobically grown Δ*cydAB* planktonic cultures,

274 raised the hypothesis that a cytochrome *bd*-expressing subpopulation exists in the

275 planktonic state under ambient oxygen conditions and that this cytochrome *bd*-

276 expressing subpopulation exhibits the greatest fitness advantage during infection. To

277 test this hypothesis, we first analyzed transcript abundance in cultures used for

278 inoculation during murine infections with qPCR and PNA-FISH (Fig. 5). Under these

279 conditions, qPCR analysis indicated that the majority of transcript corresponds to

280 *cyoABCD* (69.7%), with *cydABX* and *appBC* transcripts each comprising approximately

281 15% of detected transcripts (Fig. 5a). Transcript abundance was altered by decreasing

282 ambient oxygen concentrations, with the most abundant transcript corresponding to

283 *cydABX* in 12%, 8% and 4% oxygen, the latter being the concentration of dissolved

284 oxygen concentration in the urine (Figs. 5a-b and S4) (31). PNA-FISH analysis revealed

285 the presence of bacteria which uniquely express cytochrome *bo* (Fig. 5f)*, bd* (Fig. 5e),

286 or *bd*$_2$ (Fig. 5g), as well as some cells that have transcript of all three operons (Fig. 5c,

287 e-g). Intriguingly, we observed dividing cells in which each daughter had distinct

288 cytochrome oxidase transcript abundance (Fig. 5c, inset), suggesting that asymmetric

289 distribution of respiratory transcripts during division may be a mechanism by which

290 these subpopulations are generated.

13

291

Expression of cytochrome bd is dominant during acute urinary tract infection

293   Previous studies reported that deletion of cytochrome *bd* impairs UPEC virulence

294 in a UTI model (28). To gauge the contribution of each cytochrome oxidase during

295 infection, we evaluated the fitness of Δ*cyoAB, ΔappBC*, and Δ*cydAB* mutants compared

296 to the parent strain in a murine model of acute urinary tract infection. Consistent with the

297 previous report (28), Δ*cydAB* exhibited a ~2 log decrease in bladder colonization by 24

298 hours relative to the parent strain, while the mutants deleted for *cyoAB* and *appBC*

299 colonize mice at the same level as the parent strain (Fig. 5m). Subsequent PNA-FISH

300 on pooled urine obtained from mice infected with the parent strain revealed a marked

301 enrichment in cytochrome *bd*-expressing cells and a corresponding reduction in the

302 number of cells expressing cytochrome *bo* (Fig. 5h-l). This suggests that the bladder

303 environment either induces transcription of *cydABX* or that only subpopulations of

304 bacteria expressing *cydABX* are capable of efficiently colonizing the bladder. Together

305 these data reveal the presence of subpopulations of bacteria that differentially express

306 cytochrome oxidases as a potential bet-hedging mechanism to promote bladder

307 colonization.

308

309 **Discussion**

310   Cytochrome *bd* is a multifunctional protein that is central to respiration and can

311 maintain activity in the face of nitrosative stress (26). As such, bacteria expressing

312 cytochrome *bd* presumably exhibit a fitness advantage during growth conditions that are

14

313   low in oxygen or high in metabolic byproducts that increase nitric oxide concentration.

314   The biofilm state, while protecting the bacterial residents from predation and

315   desiccation, constitutes a high-density environment with several chemical gradients that

316   result from the consumption and production of metabolites. Accordingly, expressing an

317   enzyme that can facilitate tolerance to metabolic byproducts, such as nitric oxide, would

318   ensure that biofilm residents do not perish as a consequence of their own metabolic

319   excretions. Our study elucidates the distribution of cytochrome oxidase expression in

320   the biofilm state and indicates that the bulk of biofilm residents express cytochrome *bd*,

321   particularly in the densely populated interior. The cytochrome *bd*-expressing bacteria

322   are not necessarily using cytochrome *bd* for respiration, as many of them also have low

323   levels of cytochrome *bo* and *bd₂* transcripts (Fig. 2 and S1). Rather, the production of

324   cytochrome *bd* may be leveraged towards providing tolerance to nitrosative stress,

325   which irreversibly inhibits cytochrome *bo*. Indeed, in Δ*cydAB* biofilms we observe a

326   marked increase in cytochrome *bo* expression (Fig. S5), suggesting that loss of

327   cytochrome *bd* impairs nitric oxide tolerance and that increased production of

328   cytochrome *bo* may be a compensatory mechanism that allows biofilm bacteria to

329   respire in the presence of high levels of nitric oxide.

330   In addition to acting as a respiratory inhibitor, nitric oxide regulates cyclic di-GMP

331   abundance and thereby governs the switch from motility to aggregation and biofilm

332   expansion (37, 38). Consequently, if cytochrome *bd* decreases nitric oxide availability, it

333   would indirectly influence ECM production. Consistent with this hypothesis, loss of the

334   cytochrome *bd*-expressing subpopulation reduces the total abundance of matrix

335   components and leads to gross alterations of biofilm architecture (Fig. 3). It is thus

336   possible that the cytochrome *bd*-expressing subpopulation is critical for promoting the

337   biosynthesis of the ECM by influencing the nitric oxide – cyclic di-GMP signaling axis.

338   We are currently investigating this possibility.

339   Most importantly, this work revealed the presence of planktonic subpopulations

340   that express distinct cytochrome oxidases during growth. In conjunction with the

341   observation that only cytochrome *bd* expression is critical for fitness during infection,

342   this finding suggests that basal expression of cytochrome *bd* under aerobic conditions

343   serves as a bet-hedging mechanism that promotes the expansion of bacteria during the

344   transition from the aerobic perineum to the hypoxic bladder. In addition to allowing for

345   efficient respiration in the hypoxic bladder, expression of cytochrome *bd* provides

346   resistance against nitrosative stress – a metabolic byproduct and component of the

347   innate immune response – and promotes the formation of resilient biofilm communities.

348   These observations suggest the presence of respiratory bet-hedging behavior in UPEC,

349   and additionally suggest the possibility of targeting heterogeneity as a method for

350   homogenizing bacterial populations and impeding their ability to colonize the urinary

351   tract.

352

353   **Materials and Methods**

354   Bacterial Strains

355   All studies were performed in *Escherichia coli* cystitis isolate UTI89 (39). All gene

356   deletions (Δ*cyoAB*, Δ*appBC*, and Δ*cydAB*) were performed using the λ-red

357   recombinase system (40). Complementation constructs were created in plasmid

358   pTRC99a with *cydABX* under the control of its native promoter as previously described

359   (41). Primers used for gene deletions and complementation plasmid construction are

360   listed in Table S1.

361

362   Growth conditions

363   For all analyses, strains were propagated overnight at 37°C with shaking in Lysogeny

364   broth (LB) (Fisher) at pH 7.4. To form colony biofilms, 10 μL of overnight culture was

365   spotted onto 1.2x Yeast Extract/Casamino Acids (YESCA) agar (9) and allowed to grow

366   at room temperature. Growth curves to assess tolerance to nitrosative or oxidative

367   stress were performed in LB broth at 37°C with shaking, starting from an overnight

368   culture normalized to optical density at 600 nm (OD_{600}) = 0.05. At 2 hours post-

369   inoculation, cultures were split into equal volumes and treated with 0.5 mM NOC-12, 1

370   mM H_2O_2, or left unperturbed. OD_{600} and CFU per mL measurements were taken every

371   hour for 8 hours.

372

373   RT-qPCR

374   RNA was extracted from day 11 colony biofilms or planktonic cultures using the RNeasy

375   kit (Qiagen). RNA was DNase treated using Turbo DNase I (Invitrogen), and reverse

376   transcribed using SuperScript III Reverse Transcriptase (Invitrogen). cDNA was

377   amplified in an Applied Biosystems StepOne Plus Real-Time PCR machine using

378   TaqMan MGB chemistry with the primers and probes listed in Table S1. All reactions

379   were performed in triplicate with four different cDNA concentrations (100, 50, 25, or 12.5

380   ng per reaction). Relative fold difference in transcript abundance was determined using

17

381 the $\Delta\Delta C_T$ method (42) with target transcripts normalized to *gyrB* abundance from a total

382 of 3 – 4 biological replicates.

383

384 Peptide nucleic acid fluorescence *in situ* hybridization (PNA-FISH)

385 Day 11 biofilms were flash frozen in Tissue-Tek O.C.T. compound (Electron Microscopy

386 Sciences) and cryosectioned as described previously (5). The PNA-FISH hybridization

387 protocol was adapted from Almeida *et al* (43). Biofilm cryosections were fixed in 4%

388 paraformaldehyde (PFA) for 30 minutes at room temperature, then dehydrated for 10

389 minutes in 50% ethanol. After dehydration, 100 µL of hybridization solution (see below

390 for details) was applied to the slides. All hybridizations were performed at 60˚C for 30

391 minutes. Next, slides were submerged in pre-warmed wash solution for 30 minutes,

392 mounted using ProLong Diamond (ThermoFisher), and imaged using a Zeiss 710

393 confocal laser scanning microscope (CLSM). For planktonic cells, 1 mL of culture was

394 sedimented, fixed in 4% PFA, resuspended in 50% ethanol, incubated at -20˚C for 30

395 minutes, and resuspended in 100 µL hybridization solution. After hybridization, cells

396 were pelleted, resuspended in 500 µL pre-warmed wash solution, and incubated at

397 60˚C for 30 minutes. Finally, cells were pelleted and resuspended in 100 µL sterile

398 water before being applied to microscope slides for imaging. Wash solution contained 5

399 mM Tris-HCl pH 7.4, 15 mM NaCl, and 1% Triton X-100. Hybridization solution

400 contained 10% w/v dextran sulfate, 30% formamide, 50 mM Tris-HCl pH 7.4, 10 mM

401 NaCl, 5 mM EDTA, 0.1% Triton X-100, and 200 nM of each PNA-FISH probe. Probe

402 sequences were based on the probes used for qPCR (efficiency of hybridization: *rrsH*:

18

403   81; *cydA*: 107; *cyoA*: 115; *appC*: 73) and were synthesized by PNA Bio (Newbury Park,

404   CA).

405

406   <u>ATP measurements</u>

407   ATP was quantified from mid-log (4 hours after subculture) planktonic cultures using

408   Cell-Glo Titer kit (Promega). Cultures were normalized to OD_{600} = 0.5, pelleted, and

409   resuspended in PBS. 50 µL of bacterial suspension was mixed with an equal volume of

410   Cell-Glo Titer reagent and incubated shaking at room temperature for 15 minutes. After

411   incubation, luminescence was measured on a SpectraMax i3 plate reader (Molecular

412   Devices). Luminescence was converted to concentration of ATP using a standard curve

413   on the same plate.

414

415   <u>Extracellular matrix extraction</u>

416   Extracellular matrix was extracted using established methods (20). Briefly, biofilms were

417   grown on YESCA agar containing 25 µg/mL Congo Red. After 60 hours, biofilms were

418   homogenized in cold 10 mM Tris-HCl pH 7.4 using an Omni Tissue Homogenizer

419   (motor speed 9) five times for one minute per cycle. Next, the homogenate was

420   centrifuged three times for 10 minutes at 5,000*g* to remove cells. The supernatant was

421   spiked with NaCl (final concentration 170mM) and centrifuged for one hour at 13,000*g*

422   to pellet the matrix. The ECM pellet was washed in 10 mM Tris-HCl pH 7.4 with 4%

423   SDS and incubated at room temperature rocking overnight. Next, the suspended ECM

424   was centrifuged at 13,000*g* for one hour, resuspended in cold 10 mM Tris-HCl pH 7.4,

19

425   and centrifuged at 30,000g for 20 minutes. Pelleted ECM was resuspended in MQ water

426   and flash frozen.

427

428   <u>Solid-state NMR Measurements</u>

429   All NMR experiments were performed in an 89 mm bore 11.7T magnet using either an

430   HCN Agilent probe with a DD2 console (Agilent Technologies) or a home-built four-

431   frequency transmission line probe with a Varian console. Samples were spun at 7143

432   Hz in either 36 µL capacity 3.2 mm Zirconia rotors or thin-walled 5 mm outer diameter

433   Zirconia rotors. The temperature was maintained at 5˚C with an FTS chiller (FTS

434   Thermal Products, SP Scientific, Warminster, PA) supplying nitrogen at -10˚C. The field

435   strength for ^{13}C cross polarization was 50 kHz with a 10% ^{1}H linear ramp centered at 57

436   kHz. The CPMAS recycle time was 2 s for all experiments. ^{1}H decoupling was

437   performed with continuous wave decoupling. ^{13}C chemical shifts were referenced to

438   tetramethylsilane as 0 ppm using a solid adamantine sample at 38.5 ppm. The 15.6 mg

439   wild-type ^{13}C CPMAS spectrum was the result of 32,768 scans and the 8.3 mg mutant

440   spectrum was the result of 100,000 scans. NMR spectra were processed with 80 Hz line

441   broadening.

442

443   <u>SDS-PAGE gels</u>

444   A portion of the lyophilized ECM sample used for solid-state NMR analysis was

445   resuspended in 98% formic acid and vacuum centrifuged. The samples were then

446   reconstituted in SDS-PAGE sample buffer containing 8M urea and 50 mM DTT and

447   further diluted to desired concentrations. All samples were centrifuged briefly at 10,000g

448 to remove any insoluble material and used for electrophoresis. The gels were stained

449 with instant blue and de-stained in water.

450

451 Immunofluorescence

452 Immunofluorescence targeting CsgA, the major curli subunit, was performed as

453 previously described (10). Biofilm cryosections were fixed in 4% PFA for 30 minutes at

454 room temperature and blocked overnight in 5% BSA at 4°C. Sections were washed in

455 PBS, incubated with rabbit α-CsgA antibodies (GenScript) (1:1000) at room temperature

456 for 1 hour, washed in PBS, and incubated with AlexaFluor 647 goat α-rabbit IgG

457 (ThermoFisher) (1:1000) at room temperature for 1 hour. Slides were counterstained

458 with SYTO 9 and imaged using CLSM.

459

460 Murine infections

461 Murine infections were performed as described previously (44). In brief, UTI89 and each

462 mutant strain were inoculated individually into 5 mL LB medium and grown shaking at

463 37°C for 4 hours. Next, this culture was diluted 1:1000 into 10 mL fresh media and

464 grown statically at 37°C for 24 hours. After 24 hours, this culture was diluted 1:1000 into

465 10 mL fresh media and grown for another 24 hours at 37°C statically. Next, 7 – 8 week

466 old C3H/HeN female mice were transurethrally inoculated with 50 μL PBS containing

467 10^7 CFU bacteria. Mice were sacrificed at 24 hours post infection after which bladders

468 were removed and homogenized for CFU enumeration. All animal studies were

469 approved by the Vanderbilt University Medical Center Institutional Animal Care and

470 Use Committee (IACUC) (protocol number M/12/191) and carried out in accordance

21

471   with all recommendations in the Guide for the Care and Use of Laboratory Animals of

472   the National Institutes of Health and the IACUC.

473

474   <u>Statistical analysis</u>

475   All statistical analyses were performed in GraphPad Prism using the most appropriate

476   test. Details of test used, error bars, and statistical significance cutoffs are presented in

477   figure legends.

478

479   **Acknowledgments**

487

488   **Author Contributions**

489   CJB, ARE, and MH conceived the study, performed the experiments, analyzed the data,

490   and composed the manuscript. SAR performed the nitrosative and oxidative stress

491   assays. MJF and MMH constructed deletion mutants and complementation constructs

492   under the supervision of CJB and ARE. JRB assisted with imaging data acquisition. SD

493   and DBC performed the animal experiments along with CJB and ARE, assisted in data

494   analysis, and edited the manuscript. SHW and LC performed the extracellular matrix

495   component measurements and edited the manuscript.

496

497   **Declaration of Interests**

498   The authors declare no conflicts of interest at the time of submission of this manuscript.

499

500   **References**

501   1.   Kostakioti M, Hadjifrangiskou M, Hultgren SJ. 2013. Bacterial biofilms:

502   development, dispersal, and therapeutic strategies in the dawn of the

503   postantibiotic era. Cold Spring Harb Perspect Med 3:a010306.

504   2.   Stewart P, Franklin M. 2008. Physiological heterogeneity in biofilms, Nature

505   Reviews Microbiology.

506   3.   Nadell CD, Drescher K, Foster KR. 2016. Spatial structure, cooperation and

507   competition in biofilms. Nat Rev Microbiol 14:589-600.

508   4.   Stewart PS, Franklin MJ. 2008. Physiological heterogeneity in biofilms. Nat Rev

509   Microbiol 6:199-210.

510   5.   Vlamakis H, Aguilar C, Losick R, Kolter R. 2008. Control of cell fate by the

511   formation of an architecturally complex bacterial community. Genes Dev 22:945-

512   53.

513   6.   van Gestel J, Vlamakis H, Kolter R. 2015. Division of Labor in Biofilms: the

514   Ecology of Cell Differentiation. Microbiol Spectr 3:MB-0002-2014.

515   7.   Dragoš A, Kiesewalter H, Martin M, Hsu CY, Hartmann R, Wechsler T, Eriksen

516   C, Brix S, Drescher K, Stanley-Wall N, Kümmerli R, Kovács Á. 2018. Division of

517   Labor during Biofilm Matrix Production. Curr Biol 28:1903-1913.e5.

518   8.   Dietrich LE, Okegbe C, Price-Whelan A, Sakhtah H, Hunter RC, Newman DK.

519   2013. Bacterial community morphogenesis is intimately linked to the intracellular

520   redox state. J Bacteriol 195:1371-80.

521   9.   DePas WH, Hufnagel DA, Lee JS, Blanco LP, Bernstein HC, Fisher ST, James

522   GA, Stewart PS, Chapman MR. 2013. Iron induces bimodal population

523   development by Escherichia coli. Proc Natl Acad Sci U S A 110:2629-34.

524   10. Floyd KA, Moore JL, Eberly AR, Good JA, Shaffer CL, Zaver H, Almqvist F,

525   Skaar EP, Caprioli RM, Hadjifrangiskou M. 2015. Adhesive fiber stratification in

526   uropathogenic Escherichia coli biofilms unveils oxygen-mediated control of type 1

527   pili. PLoS Pathog 11:e1004697.

528   11. Jo J, Cortez KL, Cornell WC, Price-Whelan A, Dietrich LE. 2017. An orphan cbb_3-

529   type cytochrome oxidase subunit supports *Pseudomonas aeruginosa* biofilm

530   growth and virulence. Elife 6.

531   12. Unden G, Bongaerts J. 1997. Alternative respiratory pathways of Escherichia

532   coli: energetics and transcriptional regulation in response to electron acceptors.

533   Biochim Biophys Acta 1320:217-34.

534   13. Borisov VB, Verkhovsky MI. 2015. Oxygen as Acceptor. EcoSal Plus 6.

535   14. Borisov VB, Gennis RB, Hemp J, Verkhovsky MI. 2011. The cytochrome bd

536   respiratory oxygen reductases. Biochim Biophys Acta 1807:1398-413.

537   15.   Morris RL, Schmidt TM. 2013. Shallow breathing: bacterial life at low O(2). Nat

538   Rev Microbiol 11:205-12.

539   16.   Liu J, Prindle A, Humphries J, Gabalda-Sagarra M, Asally M, Lee DY, Ly S,

540   Garcia-Ojalvo J, Süel GM. 2015. Metabolic co-dependence gives rise to

541   collective oscillations within biofilms. Nature 523:550-4.

542   17.   Cegelski L, Pinkner JS, Hammer ND, Cusumano CK, Hung CS, Chorell E, Aberg

543   V, Walker JN, Seed PC, Almqvist F, Chapman MR, Hultgren SJ. 2009. Small-

544   molecule inhibitors target Escherichia coli amyloid biogenesis and biofilm

545   formation. Nat Chem Biol 5:913-9.

546   18.   Jurcisek JA, Brockman KL, Novotny LA, Goodman SD, Bakaletz LO. 2017.

547   Nontypeable. Proc Natl Acad Sci U S A 114:E6632-E6641.

548   19.   Rapsinski GJ, Wynosky-Dolfi MA, Oppong GO, Tursi SA, Wilson RP, Brodsky IE,

549   Tükel Ç. 2015. Toll-like receptor 2 and NLRP3 cooperate to recognize a

550   functional bacterial amyloid, curli. Infect Immun 83:693-701.

551   20.   McCrate OA, Zhou X, Reichhardt C, Cegelski L. 2013. Sum of the parts:

552   composition and architecture of the bacterial extracellular matrix. J Mol Biol

553   425:4286-94.

554   21.   Thongsomboon W, Serra DO, Possling A, Hadjineophytou C, Hengge R,

555   Cegelski L. 2018. Phosphoethanolamine cellulose: A naturally produced

556   chemically modified cellulose. Science 359:334-338.

557   22.   Hufnagel DA, Depas WH, Chapman MR. 2015. The Biology of the Escherichia

558   coli Extracellular Matrix. Microbiol Spectr 3.

559   23.   Hobley L, Ostrowski A, Rao FV, Bromley KM, Porter M, Prescott AR, MacPhee
560   CE, van Aalten DM, Stanley-Wall NR. 2013. BslA is a self-assembling bacterial
561   hydrophobin that coats the Bacillus subtilis biofilm. Proc Natl Acad Sci U S A
562   110:13600-5.

563   24.   Asally M, Kittisopikul M, Rué P, Du Y, Hu Z, Çağatay T, Robinson AB, Lu H,
564   Garcia-Ojalvo J, Süel GM. 2012. Localized cell death focuses mechanical forces
565   during 3D patterning in a biofilm. Proc Natl Acad Sci U S A 109:18891-6.

566   25.   Cutruzzolà F, Frankenberg-Dinkel N. 2016. Origin and Impact of Nitric Oxide in
567   Pseudomonas aeruginosa Biofilms. J Bacteriol 198:55-65.

568   26.   Giuffrè A, Borisov VB, Arese M, Sarti P, Forte E. 2014. Cytochrome bd oxidase
569   and bacterial tolerance to oxidative and nitrosative stress. Biochim Biophys Acta
570   1837:1178-87.

571   27.   Mason MG, Shepherd M, Nicholls P, Dobbin PS, Dodsworth KS, Poole RK,
572   Cooper CE. 2009. Cytochrome bd confers nitric oxide resistance to Escherichia
573   coli. Nat Chem Biol 5:94-6.

574   28.   Shepherd M, Achard ME, Idris A, Totsika M, Phan MD, Peters KM, Sarkar S,
575   Ribeiro CA, Holyoake LV, Ladakis D, Ulett GC, Sweet MJ, Poole RK, McEwan
576   AG, Schembri MA. 2016. The cytochrome bd-I respiratory oxidase augments
577   survival of multidrug-resistant Escherichia coli during infection. Sci Rep 6:35285.

578   29.   Borisov VB, Forte E, Davletshin A, Mastronicola D, Sarti P, Giuffrè A. 2013.
579   Cytochrome bd oxidase from Escherichia coli displays high catalase activity: an
580   additional defense against oxidative stress. FEBS Lett 587:2214-8.

581 30.   Safarian S, Rajendran C, Müller H, Preu J, Langer JD, Ovchinnikov S, Hirose T,

582   Kusumoto T, Sakamoto J, Michel H. 2016. Structure of a bd oxidase indicates

583   similar   mechanisms   for   membrane-integrated   oxygen   reductases.   Science

584   352:583-6.

585 31.   Wang ZJ, Joe BN, Coakley FV, Zaharchuk G, Busse R, Yeh BM. 2008. Urinary

586   oxygen   tension   measurement   in   humans   using   magnetic   resonance   imaging.

587   Acad Radiol 15:1467-73.

588 32.   Flores-Mireles AL, Walker JN, Caparon M, Hultgren SJ. 2015. Urinary tract

589   infections: epidemiology,   mechanisms   of   infection   and   treatment   options.   Nat

590   Rev Microbiol 13:269-84.

591 33.   Hadjifrangiskou M, Kostakioti M, Chen SL, Henderson JP, Greene SE, Hultgren

592   SJ.   2011.   A   central   metabolic   circuit   controlled   by   QseC   in   pathogenic

593   Escherichia coli. Mol Microbiol 80:1516-29.

594 34.   Floyd KA, Mitchell CA, Eberly AR, Colling SJ, Zhang EW, DePas W, Chapman

595   MR, Conover M, Rogers BR, Hultgren SJ, Hadjifrangiskou M. 2016. The UbiI

596   (VisC) Aerobic Ubiquinone Synthase Is Required for Expression of Type 1 Pili,

597   Biofilm   Formation,   and   Pathogenesis   in   Uropathogenic   Escherichia   coli.   J

598   Bacteriol 198:2662-72.

599 35.   Alteri CJ, Smith SN, Mobley HL. 2009. Fitness of Escherichia coli during urinary

600   tract   infection   requires   gluconeogenesis   and   the   TCA   cycle.   PLoS   Pathog

601   5:e1000448.

602 36.   Eberly AR, Floyd KA, Beebout CJ, Colling SJ, Fitzgerald MJ, Stratton CW,

603   Schmitz JE, Hadjifrangiskou M. 2017. Biofilm   Formation   by   Uropathogenic

604   Escherichia coli Is Favored under Oxygen Conditions That Mimic the Bladder

605   Environment. Int J Mol Sci 18.

606 37. Barraud N, Schleheck D, Klebensberger J, Webb JS, Hassett DJ, Rice SA,

607   Kjelleberg S. 2009. Nitric oxide signaling in Pseudomonas aeruginosa biofilms

608   mediates phosphodiesterase activity, decreased cyclic di-GMP levels, and

609   enhanced dispersal. J Bacteriol 191:7333-42.

610 38. Hengge R. 2009. Principles of c-di-GMP signalling in bacteria. Nat Rev Microbiol

611   7:263-73.

612 39. Mulvey MA, Schilling JD, Hultgren SJ. 2001. Establishment of a persistent

613   Escherichia coli reservoir during the acute phase of a bladder infection. Infect

614   Immun 69:4572-9.

615 40. Murphy KC, Campellone KG. 2003. Lambda Red-mediated recombinogenic

616   engineering of enterohemorrhagic and enteropathogenic E. coli. BMC Mol Biol

617   4:11.

618 41. Shaffer CL, Zhang EW, Dudley AG, Dixon BR, Guckes KR, Breland EJ, Floyd

619   KA, Casella DP, Algood HM, Clayton DB, Hadjifrangiskou M. 2017. Purine

620   Biosynthesis Metabolically Constrains Intracellular Survival of Uropathogenic

621   Escherichia coli. Infect Immun 85.

622 42. Pfaffl MW. 2001. A new mathematical model for relative quantification in real-

623   time RT-PCR. Nucleic Acids Res 29:e45.

624 43. Almeida C, Azevedo NF, Santos S, Keevil CW, Vieira MJ. 2011. Discriminating

625   multi-species populations in biofilms with peptide nucleic acid fluorescence in situ

626   hybridization (PNA FISH). PLoS One 6:e14786.

627   44.   Hung CS, Dodson KW, Hultgren SJ. 2009. A murine model of urinary tract

628   infection. Nat Protoc 4:1230-43.

629
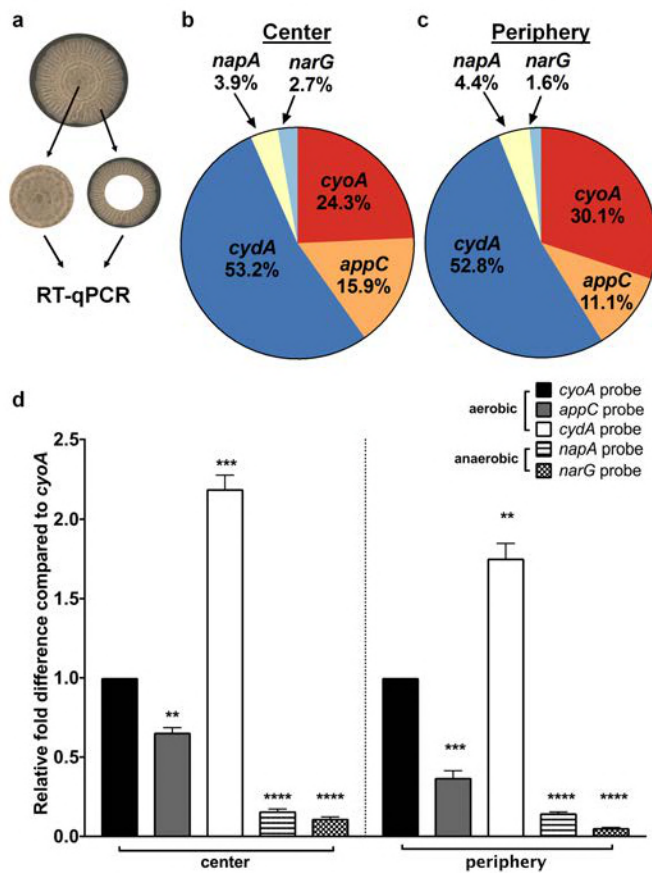
Figure 1: Lateral expression of respiratory complexes in *Escherichia coli* biofilms: a, Image of a mature colony biofilm formed by UPEC strain UTI89 on YESCA agar. The center and periphery of colony biofilms were harvested and subjected to RNA extraction and RT-qPCR using the following probes: *cydA, cyoA, appC, napA,* and *narG* with *gyrB* as a normalizer. **b – c,** Pie charts indicating the relative abundance of detected respiratory transcripts in the biofilm center (**b**) and periphery (**c**). **d,** Graphs depicting relative fold differences in transcript abundance in the biofilm center and periphery. The graph and pie chart depict the average of 4 biological replicates. Statistical analysis was performed in GraphPad Prism using a two-tailed paired t test. Data are presented as mean ± SEM. * = $p < 0.05$, ** = $p < 0.01$, *** = $p < 0.001$, **** = $p < 0.0001$.
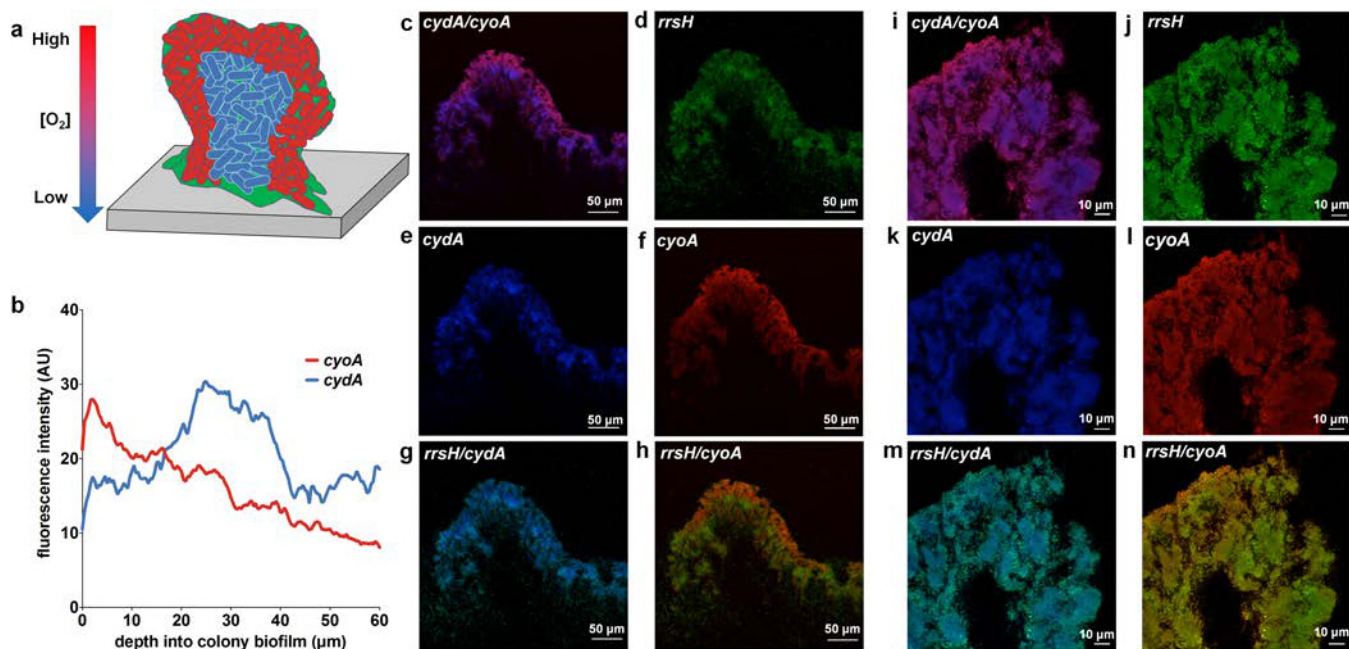
Figure 2: Expression of cytochrome oxidases as a function of the oxygen gradient. a, Cartoon depicting the detected localization of *cyoA* (red) and *cydA* (blue) transcripts in biofilm cryosections. **b,** Fluorescence intensity of *cyoA* and *cydA* PNA-FISH probes were quantified on ImageJ. Data are presented as the average fluorescence intensity as a function of depth obtained from four images, each with five measurements per image. **c – n,** Representative images of PNA-FISH stained biofilm cryosections at 20x magnification (**c – h**) and 63x magnification (**i – n**). Cryosections were stained with PNA-FISH probes targeting *cyoA* and *cydA* with *rrsH* (16S rRNA) as an endogenous control. Images are representative of three biological replicates.
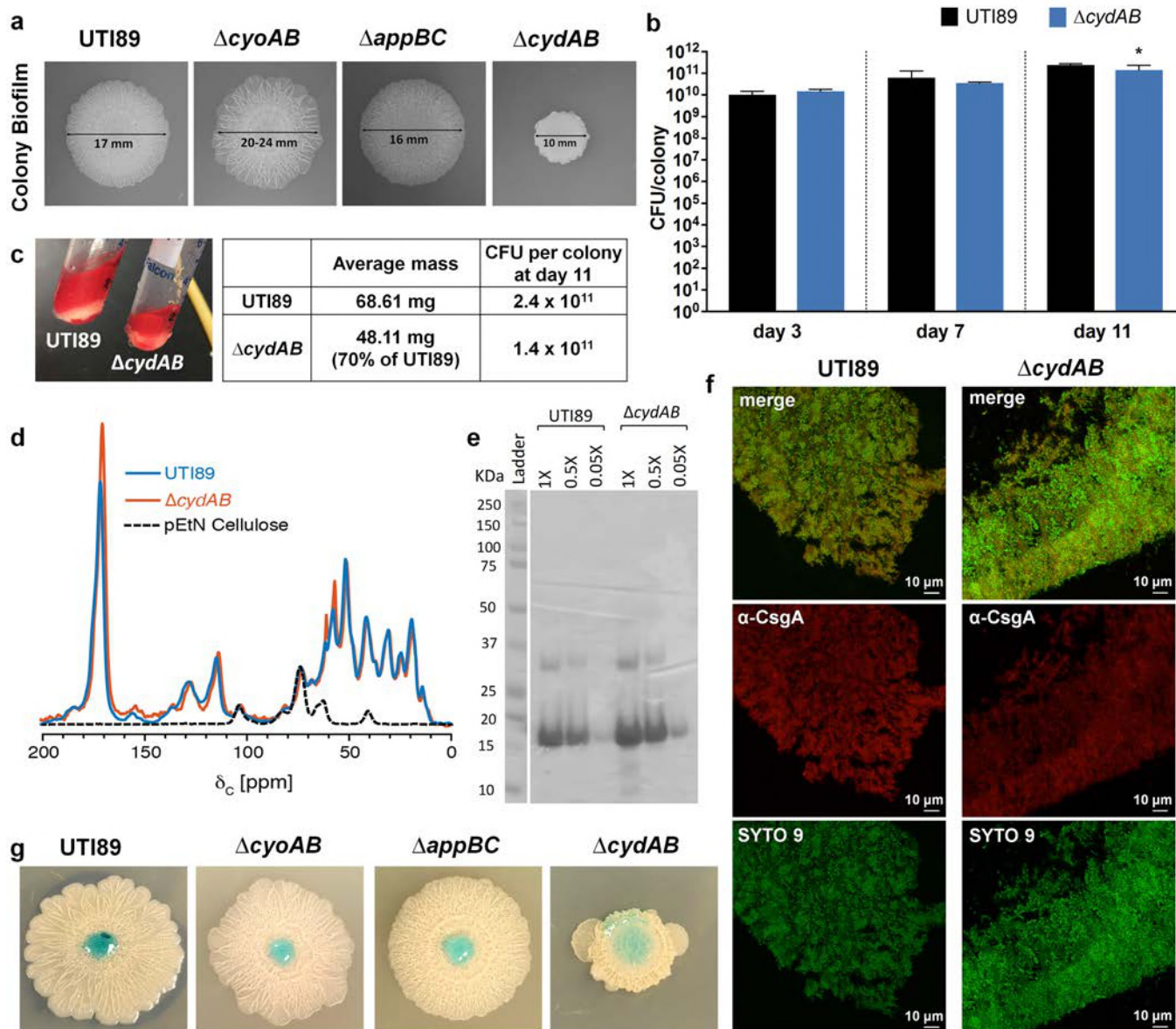
Figure 3. Cytochrome *bd* organizes biofilm architecture and ECM production. a, Colony biofilms of UTI89 and cytochrome oxidase mutants grown on YESCA agar for 11 days. Images are representative of at least 30 biological replicates. **b,** CFU per colony biofilm was measured at days 3, 7, and 11 of growth. Statistical analysis was performed in GraphPad Prism using a two-tailed unpaired t test. * = p < 0.05. Data are presented as mean ± SD. Data are representative of five biological replicates. **c, left,** Image depicting gross changes to extracellular matrix (ECM) abundance between UTI89 and Δ*cydAB* colony biofilms. ECM is stained red by the presence of Congo Red in the growth medium. **right**, Table lists average mass and CFU per colony biofilm after 11 days of growth. Average mass is from a pooled analysis of 186 individual colonies. CFU per colony is the average of five biological replicates. **d,** Solid-state NMR spectra of the ECM of UTI89 (blue), Δ*cydAB* (orange), and isolated pEtN cellulose (black). **e,** SDS-PAGE gel of UTI89 and Δ*cydAB* ECM. **f,** Immunofluorescence images of curli (α-CsgA, red) localization in UTI89 and Δ*cydAB* colony biofilm cryosections. **g,** Colored water droplets were added to the top of day 11 colony biofilms to probe biofilm barrier function.
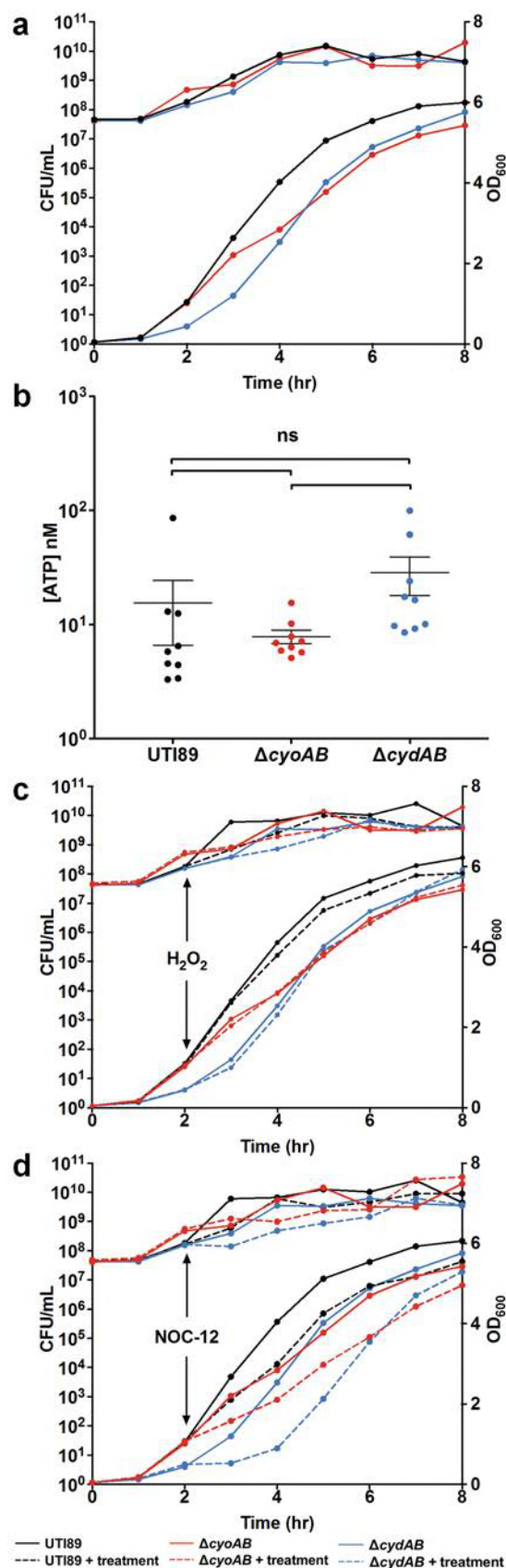
Figure 4: Cytochrome *bd* provides nitrosative stress resistance. a, Growth curves for UTI89, $\Delta cyoAB$, and $\Delta cydAB$ as measured by CFU per mL (upper lines, left axis) and OD_{600} (lower lines, right axis). **b,** ATP levels measured from logarithmic cultures of UTI89, $\Delta cyoAB$, and $\Delta cydAB$. Statistical analysis was performed on GraphPad Prism using a two-tailed unpaired t test. Data are presented as mean ± SEM. **c – d,** Growth curves for UTI89, $\Delta cyoAB$, and $\Delta cydAB$ as measured by CFU per mL (upper lines, left axis) and OD_{600} (lower lines, right axis). 0.5 mM of nitric oxide donor NOC-12 (**c**) or 1 mM hydrogen peroxide (**d**) was added at t = 2 hours. All data are representative of at least three biological replicates.
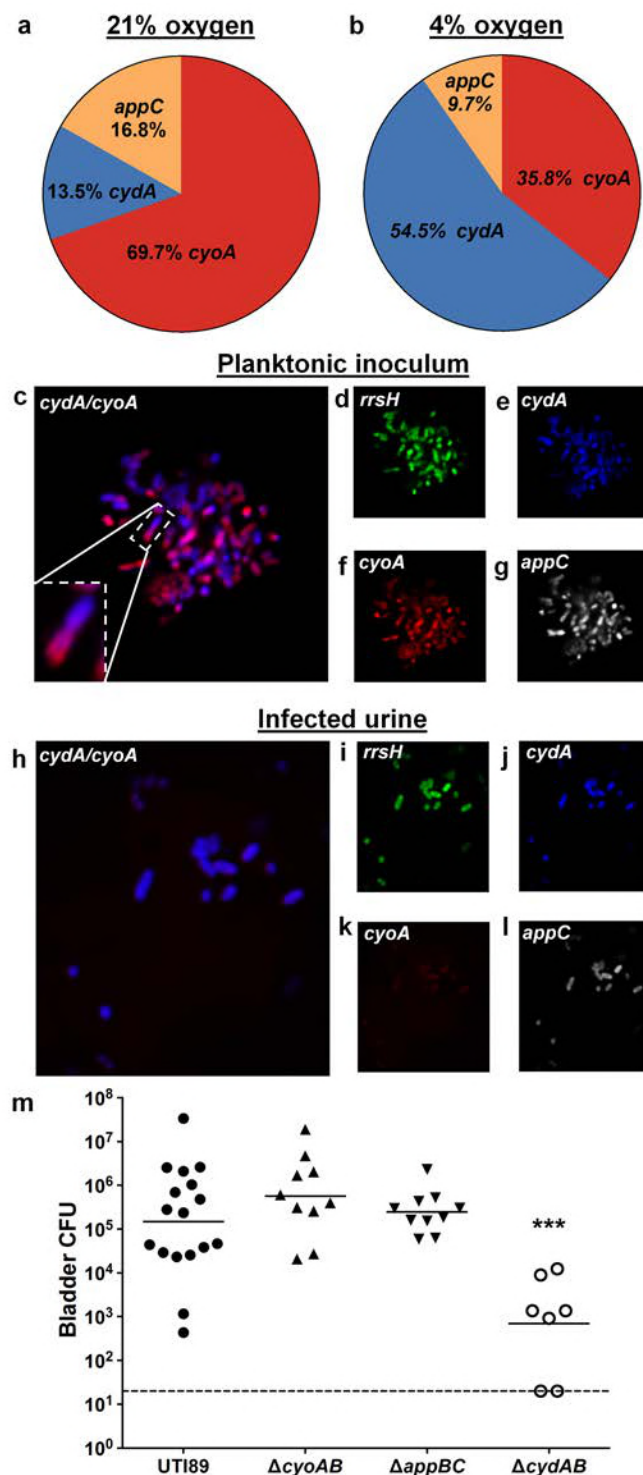
Figure 5: Respiratory heterogeneity provides a fitness advantage during urinary tract infection. a – b, Pie charts depicting relative abundance of *cydA, cyoA,* and *appC* transcripts detected using RT-qPCR in planktonic cultures grown at 21% oxygen in the manner used to prepare cultures to inoculate mice (**a**), as well as planktonic cultures grown at 4% oxygen (**b**). Data is representative of three biological replicates. **c – g,** PNA-FISH was used to detect cytochrome oxidase transcripts from cultures used to inoculate mice. Data is representative of three biological replicates. **h – l,** PNA-FISH was used to detected cytochrome oxidase transcripts in the urine of mice infected with UTI89. Urine was pooled from 20 mice. **m,** Graph depicting bladder titers obtained from mice infected with UTI89 or cytochrome oxidase mutant strains at 24 hours post infection. Each point represents a mouse. UTI89 and Δ*cydAB* are representative of two independent experiments. Δ*cyoAB* and Δ*appBC* are representative of one experiment. Statistical analysis was performed in GraphPad Prism using a two-tailed Mann-Whitney test. Line represents geometric mean. *** = p< 0.001.
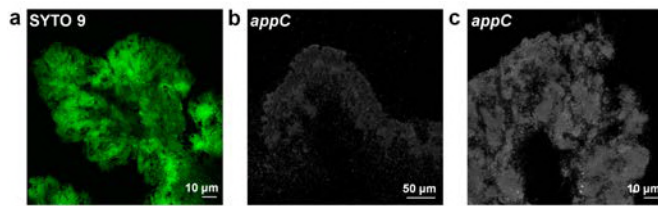
Figure S1: Localization of *appC* transcript in biofilm cryosections. a, Representative image of SYTO 9 stained biofilm cryosection at 20x magnification. **b – c,** Representative images of biofilm cryosections stained with an *appC* PNA-FISH probe at 20x (**b**) and 63x (**c**) magnification.
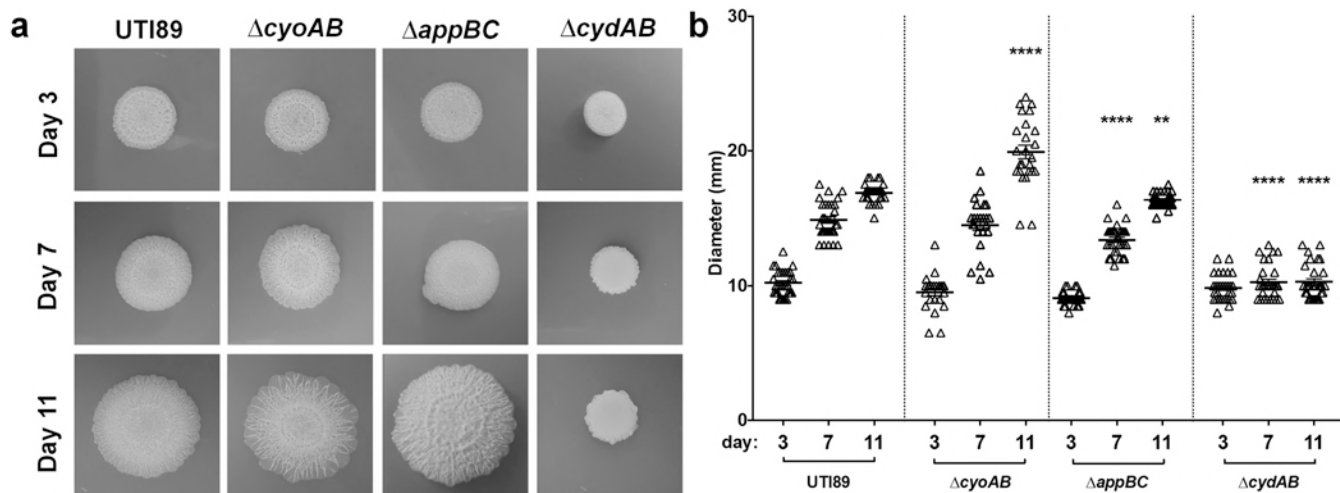
Figure S2: Temporal development of colony biofilms by UTI89 and isogenic cytochrome oxidase mutants. a, Representative images of UTI89 and cytochrome oxidase mutant colony biofilms grown on YESCA agar taken on day 3, 7, and 11 of growth. **b,** Graph depicting colony biofilm diameter at day 3, 7, and 11 of growth. Each triangle represents an individual colony biofilm. Data is representative of at least 30 biological replicates. Statistical analysis was performed in GraphPad Prism using Welch's t test. * = $p < 0.05$, ** = $p < 0.01$, *** = $p < 0.001$, **** = $p < 0.0001$.
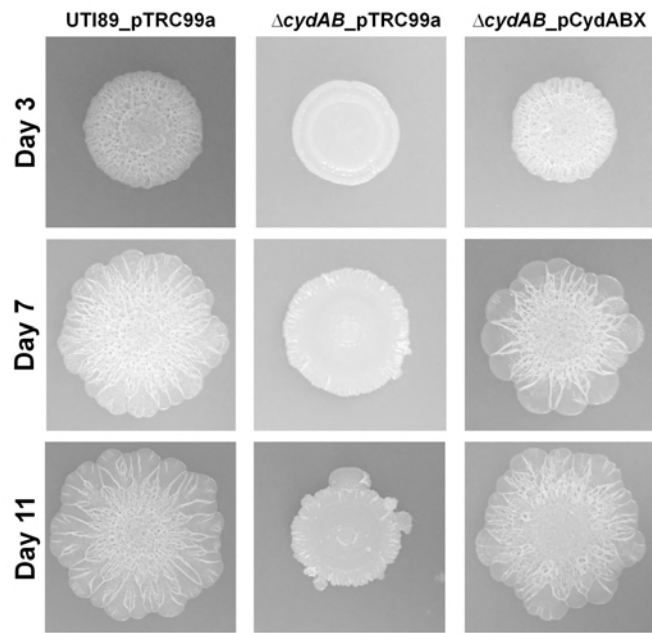
Figure S3: Extrachromosomal complementation of Δ*cydAB* rescues biofilm defects. Representative images on UTI89_pTRC99a, Δ*cydAB*_pTRC99a, and complemented Δ*cydAB*_pCydABX under the control of a native promoter. Images were taken of colony biofilms grown on YESCA agar at days 3, 7, and 11 of growth. Images are representative of at least 5 biological replicates.

Supplemental Movies S1-4: Cytochrome *bd* influences matrix hydrophobicity and resistance to penetration by aqueous solutions. Videos of colored water applied adjacent to a day 11 colony biofilm to assess the degree to which colony biofilms uptake aqueous solutions. **Movie S1,** UTI89; **Movie S2,** Δ*cyoAB*; **Movie S3,** Δ*appBC*; **Movie S4,** Δ*cydAB.* Videos are representative of at least 5 biological replicates.
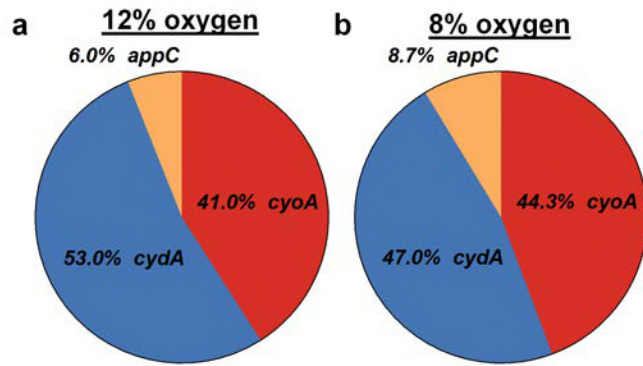
Figure S4: Ambient oxygen concentration influences cytochrome oxidase transcript abundance. Pie charts depicting relative abundance of *cydA*, *cyoA*, and *appC* transcripts detected using RT-qPCR in planktonic cultures grown at 12% (**a**) or 8% oxygen (**b**). Data is representative of three biological replicates.
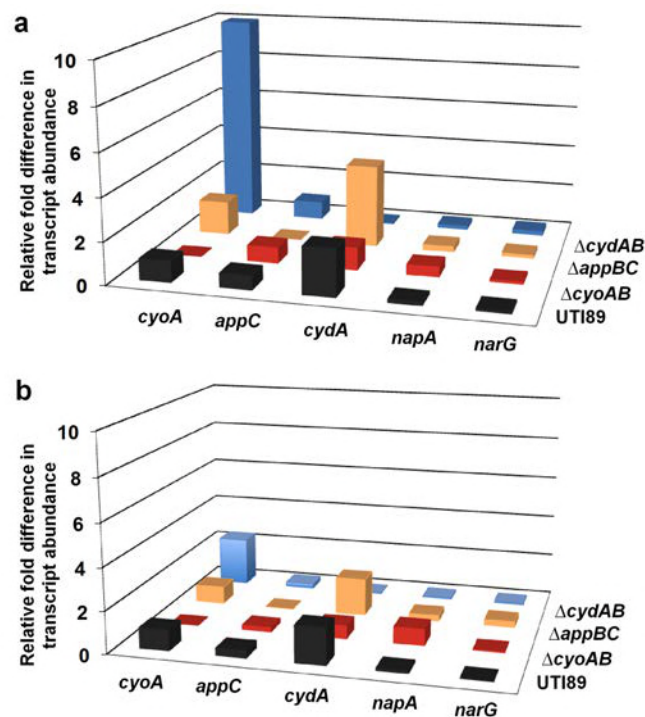
Figure S5: Expression of respiratory complexes in colony biofilms of cytochrome oxidase deletion mutants. RT-qPCR data depicting relative fold difference in respiratory transcript abundance in the center (**a**) and periphery (**b**) of day 11 colony biofilms across cytochrome oxidase mutant strains. In UTI89 (black), data is presented as relative fold difference in transcript abundance as compared to *cyoA* abundance. In each mutant strain, data is presented as relative fold difference in transcript abundance as compared to transcript abundance in UTI89.

Table S1: Primers and probes

Primer/Probe	Sequence (5' → 3')	Purpose
cydA_KO_Fwd	ATGATGTTAGATATAGTCGAACTGTCGCGCTTACAGTTT GCCTTGACCGCGATGTACGTGTAGGCTGGAGCTGCTTC	*cydAB* knockout
cydB_KO_Rev	GTTACGTTCAATATCTTCTTTGGTGATACGACCGAACATT TTCCAGTCATATGAATATCCTCCTTAG	*cydAB* knockout
cydA_KO_Test _Fwd	GATCAAATTGGTGAGATCGTGAC	*cydAB* knockout
cydB_KO_Test _Rev	CTAACAGAAGTGCCATCACG	*cydAB* knockout
cydA1_Fwd_Xb aI	CTGCAGTCTAGACTGGTCAAGTTATCCATCATTCACT	*cydABX* complementation
cydX_Rev_SacI	CGTATTGAGCTC/TTGCGATAATCTTACTCATCAGATGTC	*cydABX* complementation
appC_KO_Fwd	ATGTGGGATGTCATTGATTTATCGCGCTGGCAGTTTGCT CTGACCGCGGTGTAGGCTGGAGCTGCTTC	*appBC* knockout
appB_KO_Rev	TTAGTACAGCTCGTTTTCGTTACGGCGGAGAGTTTCTGT CGTCATGCCATATGAATATCCTCCTTAG	*appBC* knockout
appC_KO_Test _Fwd	ACGCAGACGTCACGGCG	*appBC* knockout
appB_KO_Test _Rev	TGCACAGTCAGGTGCCAGC	*appBC* knockout
cyoB_KO_Fwd	TCAGTTGCCATTTTTCAGCCCTGCCTTAGTAATCTCATC GGTGTAGGCTGGAGCTGCTTC	*cyoAB* knockout
cyoA_KO_Rev	GTCATTATTTGCAGGCACTGTATTGCTCAGTGGCTGTAA TTCTGCGCTGCATATGAATATCCTCCTTAG	*cyoAB* knockout
cyoB_KO_Test _Fwd	CATCCAGATAAGACCGGAAGTG	*cyoAB* knockout
cyoA_KO_Test _Rev	GCAACATATGTGACCTGATAGC	*cyoAB* knockout
cyoA_Fwd	CAATGCCCTGTTCCGGGTAGATG	qPCR
cyoA_Rev	ACGGTACCTATCTTAATCATCATCTTCC	qPCR
cyoA probe	NED-TCGTCGTGTGCCAGCGGCTTG	qPCR
appC_Fwd	CGATGTCGCATTACGCTCG	qPCR
appC_Rev	GGTGCAGGTTCTGTTTGCCACT	qPCR
appC probe	NED-CTGCGTATGAAGTCGCGCAAG	qPCR
cydA_Fwd	GTGGCTACCGGTCTGACCATG	qPCR
cydA_Rev	CCAACCGAAGAAGAACAGACCTAC	qPCR
cydA probe	FAM-CGCTGGCAATCGAAGGTCTGATG	qPCR
narG_Fwd	TCTCGCTATACTGGACACCTGA	qPCR
narG_Rev	CCGTATAGTCCACCGGATTCAT	qPCR
narG probe	NED-TGCCGTCTGCGCCGCAGT	qPCR
napA_Fwd	CTTCCGCGTGTGGTACTGC	qPCR
napA_Rev	GTGCCGCTCGGGATATTCC	qPCR
napA probe	FAM-CGTCTGCCTGCGGACATGGTGGTGAC	qPCR
gyrB_Fwd	GATGCGCGTGAAGGCCTGATTG	qPCR
gyrB_Rev	CACGGGCACGGGCAGCATC	qPCR
gyrB probe	VIC-ACGAACTGCTGGCGGA	qPCR
cyoA PNA	CGTCGTGTGCCA – Lys (Atto425)	PNA-FISH
cydA PNA	CGATTGCCAGCG – Lys (Cy5)	PNA-FISH
appC PNA	TGCGCGACTTCATA – Lys (TexasRed)	PNA-FISH
rrsH PNA	AGTAATTCCGATTAACG – Lys (Atto532)	PNA-FISH